Spectroscopic scanning tunnel microscopy of Cl–Si(111)7×7: Determination of Cl–Si σ^* resonance line shape

Weiming Liu, Steven Horn, Pouya Maraghechi, and S. N. Patitsas[a)]
Department of Physics, University of Lethbridge, Lethbridge, Alberta T1K 3M4, Canada

(Received 10 April 2008; accepted 8 December 2008; published 30 March 2009)

Scanning tunnel microscopy (STM) of Cl/Si(111)7×7 at low coverage has been used to carefully measure a trend with sample bias in height contrast between Cl adsorbates and silicon adatoms. The apparent height of the Cl adsorbate increases monotonically with increasing sample bias. In order to help explain the observed trend a model was developed for the tunnel current between a tungsten tip and the Si(111)7×7 surface. The model uses a tight-binding approach incorporating known local density of states information calculated using density functional theory. Simulation of the clean surface STM topography yields the correct appearance in both positive and negative sample bias. Application of the model to Cl/Si(111)7×7 allowed for a good fit to the observed contrast trend. Valuable new information on the detailed line shape of the Cl–Si σ^* antibonding resonance was obtained. Detailed knowledge of this resonance may well be crucial to future understanding of the unique long-range form of tip-induced diffusion and desorption observed on this system. © *2009 American Vacuum Society.* [DOI: 10.1116/1.3066737]

I. INTRODUCTION

The adsorption of chlorine on silicon surfaces is of great scientific importance. Cl–Si(111)7×7 has become a model system for chemisorption at both low coverage and at full monolayer coverage.[1–6] Furthermore it has been established that scanning tunnel microscopy (STM) can be used to induce diffusion and desorption of chemisorbed chlorine atoms.[7–13] This example of tip-induced diffusion is unique to our knowledge in that the effect can be achieved when the tip is not positioned directly over the adsorbate. In fact diffusion can be induced even when the tip is up to 20–30 nm away.[9–12] This very interesting and rare example of tip-induced bond-breaking warrants further study.

Chlorine adsorption of atomic chlorine on Si(111)7×7 was first studied using STM at room temperature by Villarubia and Boland.[1,2] Unoccupied states imaging showed that Cl atoms chemisorb directly on top of adatom sites. The resulting elimination of the adatom density of states (DOS) near the Fermi level causes the binding sites to appear dark compared to unreacted adatoms, for applied sample bias values of less than 1.5 V or so.[1] However, for higher bias values (>2.0 V) there is a transition to a situation where the Cl adsorbed sites appear brighter (higher) than unreacted adatoms.[1,13] The explanation for this transition has been attributed to near-resonant tunneling through the tail of a higher-lying σ^* Si–Cl antibonding state.[1] The existence of such a state is supported by the self-consistent pseudopotential band structure calculations of Schluter and Cohen. For monolayer coverage of Cl on the Si(111) surface a dispersive Si–Cl σ^* related band is found to lie from ~2.4 to 6 eV.[14] It is noted that this surface band system is quite distinct from the system studied here: a single Cl bound to an adatom of the reconstructed 7×7 surface. A detailed theoretical treatment of this system awaits.

Tip-induced diffusion of chlorine, via electron injection, is also thought to be mediated by the σ^* state. This conclusion is supported by the threshold for induced diffusion at about 2–3 eV.[9,10] It is well known that STM can be used to modify surfaces in highly controlled ways. Examples include iron atoms on cooled metal surfaces manipulated one by one to form various patterns such as quantum corrals, used to study chaos in quantum systems,[15] the reversible transfer of CO from a metal surface to the STM tip,[16] and the removal of H atoms to form atomically narrow wires on Si surfaces.[17] Multistep atom-by-atom chemical reactions involving iodobenzene (Ullman reaction) have been carried out on cold copper surfaces.[18] Also, small organic molecules can be controllably dissociated on[19,20] and dislodged from[21–23] silicon surfaces. In these examples and all other examples we know of, except for two, the tip must be extremely close to the manipulated atom or molecule before the event takes place, i.e., either right on top of the adsorbate or right beside and virtually in contact with it. An example of a slight amount of delocalized manipulation is the case of adatoms on the Si(111)7×7 surface that can have their bonding configuration altered by STM at low temperature when the tip is located in an adjacent half of the 7×7 unit cell, i.e., about 2 nm away.[24] Tip-induced diffusion and desorption of Cl/Si(111)7×7 has been shown to be possible even when the tip is located up to 20–30 nm laterally across the surface, by far a more delocalized effect.[9,10] Furthermore oscillations in the efficiency of Si–Cl bond breaking with distance have been observed.[10]

What is so special about the Si–Cl σ^* state that allows such a uniquely delocalized tip effect? Other systems are known to have resonances in the same energy range that mediate tip-induced bond breaking yet they are highly

a)Electronic mail: steve.patitsas@uleth.ca

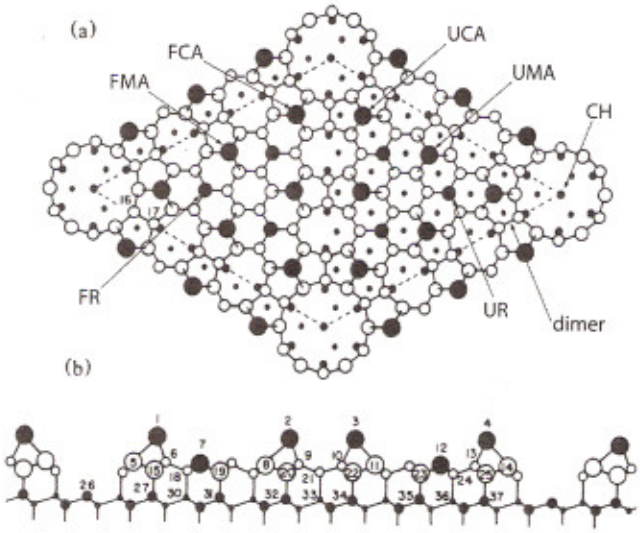

FIG. 1. Ball and stick DAS model for Si(111)7×7 unit cell shown in (a) top and (b) side view. A full unit cell with bordering area is shown. The half unit cell on the left is faulted. Large filled circles denote adatoms while medium sized filled circle denote rest atoms. Pointed out are a corner adatom on the faulted half cell (FCA), a faulted middle adatom (FMA), unfaulted corner and middle adatoms (UFA, UMA), faulted and unfaulted rest atoms (FR, UR), a corner hole (CH), and a dimer.

localized.[20–23] Here we explore whether or not there is something special about the detailed band structure, i.e., the line shape of the σ^* state. Direct probing of this state by scanning tunneling spectroscopy (STS) is complicated above ~2 V sample bias by the rapid motion of the Cl atoms. We focus only on lower bias values to avoid this problem and measure contrast between Cl sites and unreacted adatom sites in STM topographs taken over a range of sample bias values. The experimental approach taken here is unique as far as we know but is also very simple and highly reproducible. Modeling is then used to extract the σ^* DOS line shape information.

The generally accepted model for the Si(111)-7×7 surface is the dimer-adatom-stacking (DAS) fault model proposed by Takayanagi *et al.* (see Fig. 1).[25] This acceptance is largely due to a set of theoretical calculations performed by Tromp *et al.*[26] In these calculations STM images were simulated for various candidate models of the atomic structure of the surface. Comparison to the measured STM images showed striking agreement with the DAS model and all of the other models were ruled out. Although the simple approach of Tromp *et al.* was highly successful, some important effects were left out. These include density of states variations from atom to atom, the electrical field due to the STM tip, as well as relaxations of the atomic positions. Apart from the electrical field effect, these effects have been considered in the calculations by Joannopoulos and co-workers.[27–30] This group used density functional calculations for the surface wave functions. It is our goal to include all of these effects into a simple atomic orbital model, which incorporates the density functional theory (DFT) calculated density of states functions, as well as electric field effects, for the simulations of STM images of the Si(111)7×7 surface.

II. EXPERIMENT

This work was performed using a homemade STM in an ultrahigh vacuum (UHV) chamber with base pressure better than 4×10^{-11} Torr. During STM operation the chamber is continually pumped using a 300 l/s Varian StarCell ion pump as well as titanium sublimation. The STM operates at room temperature and has capabilities for both sample and tip transfer.

The silicon samples were cut from (111)-oriented wafer (*n*-type antimony doped, 0.03 Ω cm, 0.35 mm thick) purchased from Montco Silicon Technologies Inc. To remove carbon contaminants, the sample pieces were cleaned using a simplified RCA process.[31,32]

Inside the chamber the samples were heated resistively and degassed ~12 h at 640 °C before flashing at high temperatures. Sample temperatures were measured using an optical pyrometer positioned outside the vacuum chamber. The samples were flashed at 1235 °C for 10 s, while ensuring that the chamber pressure stayed lower than 2×10^{-10} Torr, followed by a quick cool down. Shortly after, they were again heated to 920 °C and then slowly cooled down at the rate of 0.5 °C/s, before transfer to the STM. The cleanliness and quality of the reconstruction and terrace structure of the surface produced by this procedure is sufficient for conducting basic studies of adsorbates with STM.

Tips were made from 0.375 mm diameter polycrystalline tungsten wire, prepared by electrochemical etching in 2.5*M* NaOH solution. Before using the tips for scanning, the tips were cleaned under UHV conditions by electron bombardment from a nearby tantalum filament. The cleanliness and sharpness of the tip were characterized by monitoring the stability and magnitude of the field emission current from the tip.[32]

Reagent grade (Merck) trichloroethylene (99.5% purity) was placed in a quartz glass tube connected to a stainless steel gas line and was repeatedly degassed by freeze-pump-thaw cycles. The clean silicon sample was exposed by passing trichloroethylene vapor into the main chamber from the gas line via a precision variable leak valve.[13]

It has been shown that at exposure of Si(111)7×7 to trichloroethylene at room temperature results in thermal dissociation of the molecule into an atomic chlorine product and a chlorovinyl group.[13] At very low dosage levels, both products chemisorb and are left separated with an average distance of 30 Å. At this level of separation the chlorine atoms can considered to be isolated, i.e., with very little effect from other adsorbates. Doses at a level of 0.1 L result in a surface with isolated chemisorbed Cl atoms suitable for STM studies.

III. THEORY

The starting point for our model of the STM tunneling current is the theory of Tersoff and Hamann,[33] which in turn builds on Bardeen's first order transport theory.[34] A key assumption is that the tip wave function has *s*-orbital symmetry and is centered on a sphere of radius R_0, which is typically referred to as the tip radius, i.e., the effective radius of cur-

vature of the end of a real STM tip. Selloni *et al.* adapted this approach to the case where the applied bias is not small so that an energy integral over density of states functions is required.[35] With this energy integration included the expression for the tunnel current is[36,37]

$$I = 16e\frac{\hbar^3\pi^3}{m^2}R_0^2\exp(\kappa R_0)n_T\int_{\varepsilon_F}^{\varepsilon_F+eV} n_S(\varepsilon - eV,\vec{r}_0)d\varepsilon, \quad (1)$$

where $\kappa=\hbar^{-1}(2m\phi)^{1/2}$ is the inverse decay length for tip wave functions in vacuum, and ϕ is the work function of the tip. In this expression the per volume density of states function for the tip n_T is assumed to be constant. Since the Tersoff-Hamann theory assumes s-wave symmetry for the tip wave function, one should count the s and p_z orbital contributions but not the lateral p_x and p_y contributions. This proper 3:1 weighting can be accomplished using tabulated calculations for separate s and p density of states functions of bulk tungsten.[38] In Eq. (1) the sample local density of states n_s evaluated at the tip position is integrated between the tip and sample Fermi levels, which are separated by the applied bias eV. Ordinarily the integral involves Fermi-Dirac distributions for both sample and tip electrons. However, since applied bias levels on the order of 1 eV are much larger than k_BT/e at room temperature the zero-temperature result of Eq. (1) is used. Equation (1) allows for voltage-dependent modeling and this approach has been used to model interesting gallium to arsenic contrast observed by STM results on GaAs(110).[39]

Evaluation of sample wave functions at the position of the tip includes the electron tunneling effect through the vacuum region separating the tip and the sample. In terms of sample wave functions the sample local density of states is given by

$$n_S(\varepsilon,\vec{r}_0) = \sum_{i,\vec{k}} |\psi_{i,\vec{k}}|^2\delta(\varepsilon - \varepsilon_i(\vec{k})), \quad (2)$$

where i is the band index and $\vec{k}$ is the wavenumber. We first develop our extension of the Tersoff and Hamann theory for the case of a monatomic Bravais unit cell. The sample wave function can be expanded into a series of atomic wave functions, ϕ_i, centered at our Bravais surface lattice sites labeled by $\vec{R}$,

$$\psi_{i,\vec{k}}(\vec{r}_0) = c\sum_{\vec{R}} e^{i\vec{k}\cdot\vec{R}}\phi_i(\vec{r}_0 - \vec{R}). \quad (3)$$

Squaring the wave function and separating out the same site contribution gives

$$|\psi_{i,\vec{k}}(\vec{r}_0)|^2 = |c|^2\sum_{\vec{R}} |\phi_i(\vec{r}_0 - \vec{R})|^2 + |c|^2\sum_{\vec{R}}\sum_{\vec{R}\neq\vec{R}} e^{i\vec{k}\cdot(\vec{R}-\vec{R}')}\phi_i(\vec{r}_0 - \vec{R})\phi_i^*(\vec{r}_0 - \vec{R}'). \quad (4)$$

When the tight-binding approximation is valid, the terms in the second summation of Eq. (4) are small because they contain the product of two atomic wave functions centered at different sites. Here we make a key assumption, i.e., by dropping these off-center terms, which leaves:

$$|\psi_{i,\vec{k}}(\vec{r}_0)|^2 \approx |c|^2\sum_{\vec{R}} |\phi_i(\vec{r}_0 - \vec{R})|^2. \quad (5)$$

Since the dropped terms are essentially what give the width or dispersion of a given band then our assumption can be considered to be fairly accurate if it is applied to cases where the modeled bands are narrow. The tight-binding approach has been successfully used in modeling STM of the Si(113)3×2 surface.[40] If N atomic sites are involved in our problem, the normalization constant c is given by

$$|c|^2 = \frac{1}{N}. \quad (6)$$

Combining Eqs. (2), (5), and (6) leads to

$$n_S(\varepsilon,\vec{r}_0) = \sum_i\sum_{\vec{R}} |\phi_i(\vec{r}_0 - \vec{R})|^2\frac{1}{N}\sum_{\vec{k}}\delta(\varepsilon - \varepsilon_i(\vec{k})). \quad (7)$$

We define

$$g_i(\varepsilon) = \frac{1}{N}\sum_{\vec{k}}\delta_{\vec{k}}(\varepsilon - \varepsilon_i(\vec{k})) \quad (8)$$

as the normalized DOS for band i (note $\int_{-\infty}^{\infty}g_i(\varepsilon)d\varepsilon=1$) so that

$$n_S(\varepsilon,\vec{r}_0) = \sum_i g_i(\varepsilon)\sum_{\vec{R}} |\phi_i(\vec{r}_0 - \vec{R})|^2. \quad (9)$$

Equation (9) is readily generalized to the case where the primitive surface unit cell contains more than one atom,

$$n_S(\varepsilon,\vec{r}_0) = \sum_{i,\alpha} g_{i,\alpha}(\varepsilon)\sum_{\vec{R}} |\phi_{i,\alpha}(\vec{r}_0 - \vec{R} - \vec{d}_\alpha)|^2. \quad (10)$$

In our model the position vector $\vec{d}_\alpha$ is used to label the atoms in the Si(111)7×7 unit cell, i.e., adatoms, rest atoms, dimers, backbonded atoms, etc. For example, consider the rest atom band. Energetically this is known to be a narrow band that lies about 0.8 eV below the Fermi level. This information is encoded into the $g_i(\varepsilon)$ function. The summation over the index α runs over the six rest atoms located in the 7×7 unit cell. In this case each $\vec{d}_\alpha$ vector points to the same wave function $\phi_{i,\alpha}$, each with the same local density of states function. To describe the sample wave function at each atomic position, atomic hydrogenlike functions are used. For silicon atoms and chlorine atoms these are the $n=3$, s, p_x, p_y, and p_z functions. For example,

$$\varphi_{3p_z} = \frac{\sqrt{2}}{81\sqrt{\pi}}\left(\frac{Z_{\text{eff}}}{a_0}\right)^{3/2}\left(6 - \frac{Z_{\text{eff}}r}{a_0}\right)\left(\frac{Z_{\text{eff}}r}{a_0}\right)\left(\frac{z}{r}\right) \times\exp\left(-\frac{Z_{\text{eff}}r}{3a_0}\right). \quad (11)$$

The hydrogenlike functions provide a good starting point since they are properly normalized and they include the proper number of radial oscillations and nodes. Roughly

speaking, they do a good job of setting the "size" of the orbital. This would be important in differentiating between a chlorine and an iodine adsorbate for example. The parameter Z_{eff} is calculated using Slater's rules[41] and takes values of 4.15 for Si and 5.75 for Cl. Hybrid orbitals are readily formed from functions such as in Eq. (11). For example a [111] oriented dangling bond orbital is expressed as

$$\varphi_{111} = \tfrac{1}{2}(\varphi_{3s} + \varphi_{3p_x} + \varphi_{3p_y} + \varphi_{3p_z}). \tag{12}$$

These functions are also easy combined to form molecular orbitals suitable for describing backbonds and dimer bonds.

The hydrogenlike wave functions are not expected to have the correct exponential decay far away from the atomic center since these functions do incorporate any surface effects. For this reason the functions are treated differently outside of the classical turning point radius, i.e., beyond which the function decays instead of oscillating. Outside the turning point we change the potential function from a Coulomb potential to a function that accurately describes the potential in the vacuum region between tip and sample. The potential function $V(r)$ developed by Pitarke *et al.* is used here.[42] This potential incorporates the long-range image force effect as well as short range interface effects such as discussed by Lang.[43] Applied bias between sample and tip is also incorporated naturally into the potential function. This is important in order to accurately calculate variations with applied bias (with varying electric field) of STM images. The potential function of Pitarke *et al.* is also attractive by being quickly evaluated numerically, requiring only the evaluation of the digamma special function.[44] Effects of the image potential are very pronounced near both interfaces and the applied bias is reflected by the asymmetry and positive slope at the midpoint between tip and sample. The Wentzel-Kramers-Brillouin (WKB) approximation is used to calculate the wave function variation through the tunnel gap. The prescription we use means replacing the exponential factor, $\exp(-Z_{\text{eff}}r/3a_0)$ in Eq. (11) with the WKB factor, $\exp(-\kappa r)$, where

$$\kappa = \sqrt{\frac{2m(V(r)-\varepsilon)}{\hbar^2}}. \tag{13}$$

Note that the WKB factor does depend on the electron energy, ε, so that lower energy states have less weight in the tunnel current because of a faster decaying wave function.

For the local density of states functions for each surface band $g_i(\varepsilon)$, the DFT calculated functions of the Joannopoulos group have been used.[28–30] This includes detailed local density of states (LDOS) functions for the four distinct types of adatoms (unfaulted corner, unfaulted middle, faulted corner, and faulted middle), the rest atoms (faulted and unfaulted), and the corner holes. In all these cases we have found that very good fits to the calculated LDOS functions are found using Gaussian functions, either one or two, of the following form:

TABLE I. Local density of states fit parameters for the most relevant surface states of the Si(111) 7×7 surface. Parameters (peak, position, standard deviation, and weight factor) are used in Gaussian function fits. For rest atom and corner hole states only one Gaussian function is required so the second set of fit parameters is not applicable (NA).

Bond type	ϵ_1 (eV)	σ_1 (eV)	w_1	ϵ_2 (eV)	σ_2 (eV)	w_2
UCA db	−0.31	0.16	0.83	0.22	0.16	0.97
UMA db	−0.28	0.16	0.587	0.28	0.16	0.907
FCA db	−0.31	0.19	1.1	0.28	0.13	0.79
FMA db	−0.31	0.138	0.63	0.20	0.216	1.11
UR db	−0.80	0.14	1.0	NA	NA	0
FR db	−0.80	0.14	1.0	NA	NA	0
CH db	−0.25	0.5	1.0	NA	NA	0
Dimer bond	−1.75	0.75	1.0	1.75	0.75	1.0
Adatom backbond	−1.75	0.75	1.0	1.75	0.75	1.0
Rest atom backbond	−1.75	0.75	1.0	1.75	0.75	1.0

$$g_i(\varepsilon) = w_i \frac{1}{\sigma_i\sqrt{2\pi}} \exp\left(\frac{-(\varepsilon-\varepsilon_1)^2}{2\sigma_1^2}\right) + w_2 \frac{1}{\sigma_2\sqrt{2\pi}} \exp\left(\frac{-(\varepsilon-\varepsilon_2)^2}{2\sigma_2^2}\right). \tag{14}$$

For adatom dangling bonds the Gaussian peaks are both centered near the Fermi level with significant overlap. The standard deviations of these Gaussian functions are small, on the order of 0.15 eV, which justifies the narrow band approximation that led to Eq. (5). A complete listing of parameters used in our model calculations is displayed in Table I. STM is highly surface sensitive so we expect the adatom dangling bond states to make the greatest contributions to the tunneling current. Adatom backbonds, although situated further from the STM tip, may make significant contributions to the tunnel current especially at higher bias values since the density of backbond states peak around ±1.8 eV as determined by STS, ultraviolet photoemission spectroscopy, and inverse photoemission spectroscopy.[45–49] Peak widths are not known but given the strong coupling of the backbonds to bulk Si there should be substantial broadening. We have chosen 0.75 eV as the standard deviation of the backbond peaks. The same parameters are used for the dimer bonds.

The DFT calculations allowed for relaxation of atomic positions for energy minimization. The equilibrium relaxations are in both the vertical and lateral directions and have been clearly tabulated.[27,28] These relaxations have been directly incorporated into our model.

IV. RESULTS AND DISCUSSION

A. Testing the theoretical model

Basic results of the STM modeling are shown in Fig. 2. Figure 2(a) shows an experimental image taken at −0.7 V with a simulated image (b) calculated at the same bias. A tip radius value of R_0=1.0 Å was chosen along with a constant tunnel current value of 10 nA. Although this set-point cur-

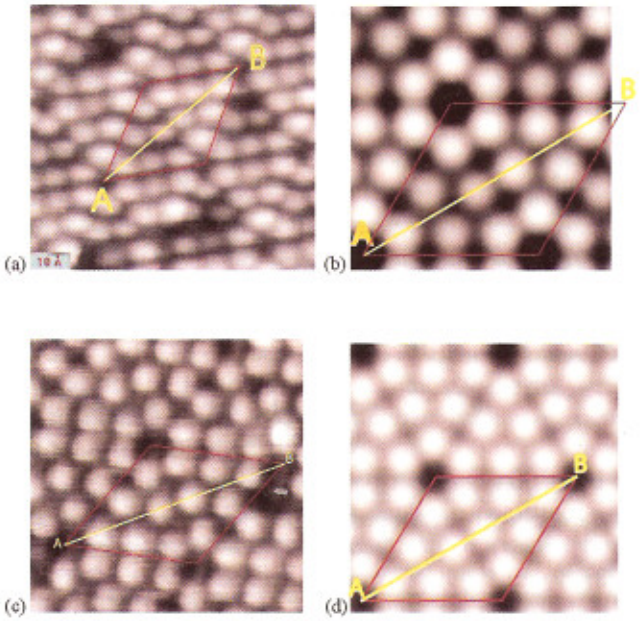

FIG. 2. (Color) [(a) and (b)] Experimental and [(b) and (d)] simulated STM topographs of occupied states at [(a) and (b)] −0.7 V bias and [(c) and (d)] unoccupied states at +1.5 V. In each image a unit cell is outlined. Also a line segment, *AB*, joins two adjacent corner holes. Starting from point *A*, the segment travels first through the unfaulted half unit cell, then the faulted half cell.

rent is about 20 times higher than experimental set point, in the model the typical tip to adatom distance has a very reasonable value of about 7 Å. Qualitatively, the agreement with experiment is very good. The most pronounced features are the adatoms and the corner hole with no noticeable contribution from the rest atoms, which is the expected result for topographic mode STM. The atoms in the unfaulted half of the unit cell (near A) are clearly less bright than those of the faulted half (near B), which is a well-known phenomenon attributed mainly to charge transfer.[45,50] This effect is also observed in the model image though less pronounced. Corner adatoms are also brighter than the middle adatoms of the same half cell, again a result attributed to charge transfer effects[45] and this effect is seen in both the experimental and simulated images.

A similar experimental to theoretical comparison is shown in Figs. 2(c) and 2(d) at unoccupied states. Here adatoms again play the major role and in this case the situation is very simple with all adatoms appearing to have approximately the same height in both images. In this case the average height of the faulted adatoms is ~0.04 Å higher[27] than the average unfaulted adatom height but this is almost exactly offset by electronic structure contrast.

A quantitative comparison between theory and experiment is summarized in Fig. 3 where actual height differences between adatoms is displayed. Since absolute heights are not obtainable experimentally atom heights are referenced to the unfaulted corner adatom in all cases. For example, Fig. 3(a) shows that experimentally, at −0.7 V sample bias, the unfaulted middle adatoms appear to lie 0.3 Å lower than the unfaulted corner adatoms. Theoretically the level of contrast

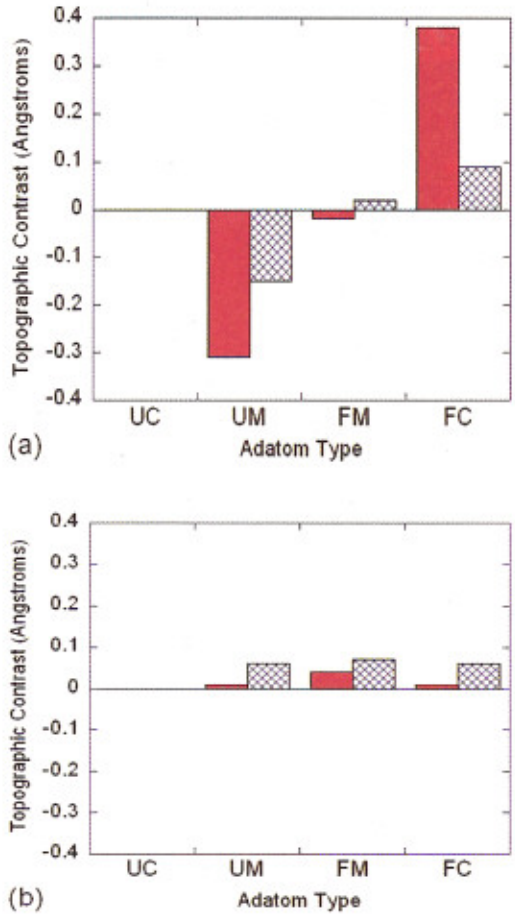

FIG. 3. (Color) Quantitative comparison of relative adatom heights. All adatom heights are referenced to the unfaulted corner (UC) adatom heights. Solid red (cross-hatched blue) bars denote experimental (theoretical) contrast values. Occupied states data are presented in (a) while unoccupied state data are shown on the same scale in (b). Typical uncertainties are ±0.03 Å.

is only half this amount. For the case of the faulted middle adatom the agreement between experiment is theory is good while for the case of the faulted corner adatom, the model fails to achieve the large level of contrast seen in the experimental topographs.

In unoccupied states, the agreement between theory and experimental adatom contrasts is quite good, within ~0.05 Å in all cases. Error bars for the experiments are judged to be 0.03 Å, with variations in tip conditions making the largest contribution. Thus we conclude that the model calculation is quite accurate when dealing with unoccupied states. In the analysis which follows modeling will be focused on results taken of unoccupied states only.

B. Chlorine atom to adatom contrast

Figure 4 shows STM images taken at room temperature after a low dose of TCE. In (a)–(c) yellow arrows point to isolated chlorine atoms chemisorbed on top of adatoms. Cl–Si contrast is large at +2.0 V sample bias, lesser but still positive at +1.7 V and negative at +1.0 V. Dozens of similar images over a bias range from 0.8 to 2.0 V were analyzed and the Cl–Si contrast results have been averaged and dis-

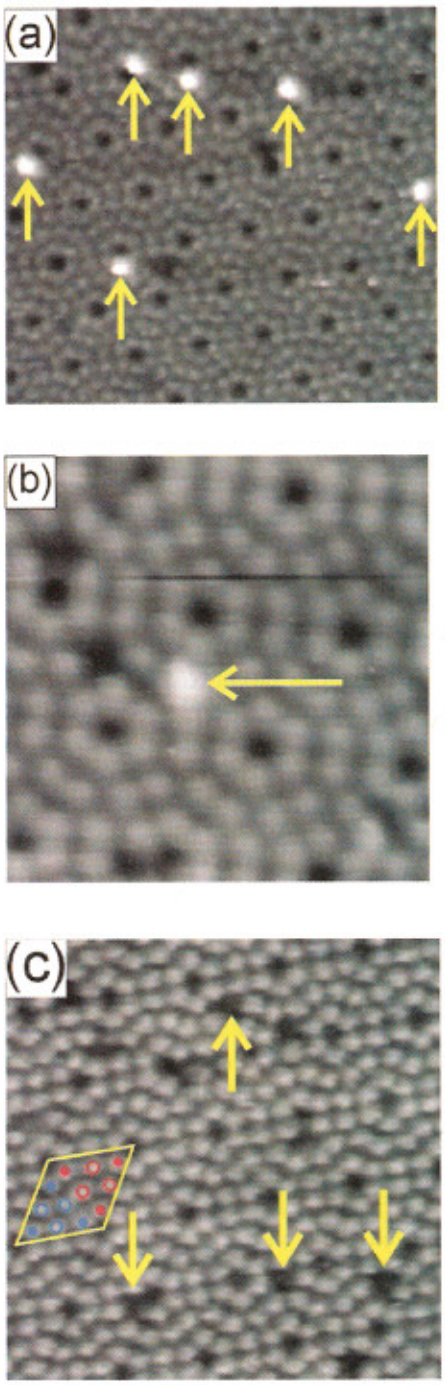

FIG. 4. (Color) STM images showing chlorine to silicon adatom contrast. Unoccupied state STM topographs of chlorine dosed Si(111)7×7 surface at (a) +2.0 V, (b) +1.7 V, and (c) +1.0 V sample biases. Chemisorbed chlorine atoms, indicated with arrows, appear as [(a) and (b)], bright and (c) gray features on top of adatoms depending on the applied bias. One unit cell is outlined in yellow. Filled (open) circles label corner (middle) adatoms and red (blue) markers denote (un)faulted adatoms.

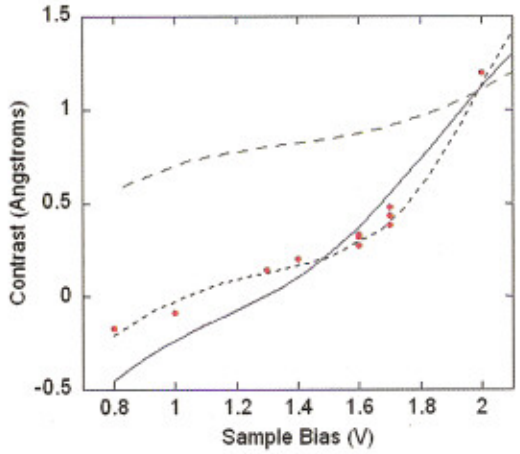

FIG. 5. (Color) Chlorine to silicon adatom contrast as a function of sample bias. Experimental data are presented as solid red circles. Vertical error bars (not shown) are ±0.03 Å. Three theoretical fit curves are shown using Lorentzian line shape (green dashed) with parameters, ε_P=2.5 eV, δ =0.4 eV, Gaussian line shape (solid blue) with parameters, ε_P=2.5 eV, σ =0.4 eV, and Voigt line shape (black short dashed) with parameters, ε_P =2.33 eV, σ=0.23 eV, and δ=0.032 eV.

played in Fig. 5. At 1.6 V (and at 1.7 V) we have displayed three data points each taken with a different tip on a different run. Although vertical error bars are difficult to quantify, given the variation between different tips demonstrated by the multiple data points at 1.6 and 1.7 V we nominally assign an uncertainty of ±0.03 Å. Despite these small tip effects a clear trend is observed from a modest amount of negative contrast at low bias values to large positive contrast at +2.0 V above which tip-induced Cl diffusion is rapid. As discussed above, this curve must contain information about the σ^* state. The approach taken here is to place a Cl atom 2.03 Å above a Si adatom[51] and input an antibonding orbital with a certain line shape into our model.

Our first choice for a line shape fitting function was the Lorentzian, i.e.,

$$L(\varepsilon) = \frac{\delta}{\pi} \frac{1}{(\varepsilon - \varepsilon_P)^2 + \delta^2} \tag{15}$$

with peak position ε_P and width parameter δ. This is the natural choice since it results from the simple coupling of an isolated energy level with a large dissipative system.[52] After inputting this function into the model and varying parameters over a wide range of reasonable choices we were unable to arrive at a good fit to our data. Essentially the Lorentzian line shape has too much weight far away from the peak. In fact there is so much weight at energies around +1.0 eV (>1 eV away from peak position) that negative contrast simply cannot reasonably be achieved. This is a significant result: detailed information about the line shape of a surface resonance can be obtained simply from measuring relative height trends in standard STM topographs.

Assuming a Gaussian line shape

$$G(\varepsilon) = \frac{1}{\sigma\sqrt{2\pi}} \exp\left(\frac{-(\varepsilon - \varepsilon_P)^2}{2\sigma^2}\right) \tag{16}$$

did result in negative contrast at bias levels lower than about 1.2 V. This could be expected since the tail of the Gaussian distribution falls off more rapidly than the Lorentzian. Although parameters ε_P and σ could be chosen to give an adequate overall fit the theoretical curve always lies too low at low bias and too high at higher bias. In this case the Gauss-

ian line shape falls off too quickly. In order to arrive at a better fit a Voigt function[53] was then used, i.e., a convolution of the previous line shape functions,

$$V(\varepsilon) = \int_{-\infty}^{\infty} G(\varepsilon')L(\varepsilon - \varepsilon')d\varepsilon'. \quad (17)$$

This function is specified by three parameters and can be calculated quickly using a polynomial-based approximation scheme.[54] With enough adjustable parameters a good least-square fit was obtained with the following values: $\varepsilon_P = 2.33$ eV, $\sigma = 0.23$ eV, and $\delta = 0.032$ eV. This is a line shape function that is mostly Gaussian with some extra weight pushed out into the tail to give the correct amount of contrast in the 0.8–1.0 V range.

As far as we know there is no fundamental reason for having a Voigt line shape for an antibonding surface resonance. Coupling of a discrete energy level to a continuum of states with constant density is known to result in a Lorentzian lineshape.[52] Since the DOS for silicon is not constant we may think of the Voigt line shape as a correction, i.e., an approximation to the true line shape. We feel that given the lack of any previous theoretical knowledge of the σ^* state this is a reasonable approach, and that one should view the above analysis as an empirical determination of the shape of the low energy tail of the Cl–Si σ^* resonance.

V. SUMMARY

In summary, STM of Cl/Si(111)7×7 has been used to measure height contrast between Cl adsorbates and silicon adatoms over a wide range of positive sample biases. A clear trend with bias was observed with a transition occurring around +1.4 eV. In order to ascertain the cause of the observed trend a model was developed for the tunnel current between a tungsten tip and the Si(111)7×7 surface. Starting from the Tersoff-Hamman theory a tight-binding extension was developed that allows for simulation of STM images at variable bias. The tight-binding approximation is well suited to simulate tunneling from the narrow surface bands that dominate the STM images of this surface. Simulation of the clean surface yields the correct appearance in both positive and negative sample bias. In unoccupied states the adatom contrasts are in good quantitative agreement with experiment.

Addition of chlorine to the model allowed calculation of the Cl–Si contrast as a function of sample bias. To our knowledge, this is the first theoretical electronic structure study of the isolated chlorine/Si(111)7×7 adsorbate. Data fitting with Lorentzian line shape was very poor. Somewhat better fitting was obtained with a Gaussian line shape while use of a Voigt line shape resulted in an adequate fit. At positive sample bias the Cl to Si topographic contrast is very sensitive to the tail of the Cl–Si σ^* antibonding resonance. Detailed knowledge of this tail may well be crucial to future understanding of the unique long-range form of tip-induced diffusion and desorption observed on this system.

ACKNOWLEDGMENTS

The authors acknowledge the National Sciences and Engineering Research Council of Canada (NSERC) for their support of this work, as well as Cathy J. Meyer for her careful reading of the manuscript.

[1] J. S. Villarrubia and J. J. Boland, Phys. Rev. Lett. **63**, 306 (1989).
[2] J. J. Boland and J. S. Villarrubia, Science **248**, 838 (1990).
[3] X. H. Chen, J. C. Polanyi, and D. Rogers, Surf. Sci. **376**, 77 (1997).
[4] C. M. Aldao and J. H. Weaver, Prog. Surf. Sci. **68**, 189 (2001).
[5] B. J. Eves and G. P. Lopinski, Surf. Sci. Lett. **579**, L89 (2005).
[6] M. Baba and S. Matsui, Appl. Phys. Lett. **64**, 2852 (1994).
[7] M. Baba and S. Matsui, Appl. Phys. Lett. **65**, 1927 (1994).
[8] M. Baba and S. Matsui, J. Vac. Sci. Technol. B **12**, 3716 (1994).
[9] Y. Nakamura, Y. Mera, and K. Maeda, Surf. Sci. **487**, 127 (2001).
[10] Y. Nakamura, Y. Mera, and K. Maeda, Phys. Rev. Lett. **89**, 266805 (2002).
[11] Y. Nakamura, Y. Mera, and K. Maeda, Surf. Sci. **497**, 166 (2002).
[12] Y. Nakamura, Y. Mera, and K. Maeda, Surf. Sci. **601**, 2189 (2007).
[13] P. Maraghechi, S. A. Horn, and S. N. Patitsas, Surf. Sci. Lett. **601**, L1 (2007).
[14] M. Schlüter and M. L. Cohen, Phys. Rev. B **17**, 716 (1978).
[15] M. F. Crommie, C. P. Lutz, and D. M. Eigler, Science **262**, 218 (1993).
[16] L. Bartels, G. Meyer, K.-H. Rieder, D. Velic, E. Knoesel, A. Hotzel, M. Wolf, and G. Ertl, Phys. Rev. Lett. **80**, 2004 (1998).
[17] T.-C. Shen, C. Wang, G. C. Abeln, J. R. Tucker, J. W. Lyding, Ph. Avouris, and R. E. Walkup, Science **268**, 1590 (1995).
[18] S.-W. Hla, L. Bartels, G. Meyer, and K.-H. Reider, Phys. Rev. Lett. **85**, 2777 (2000).
[19] P. H. Lu, J. C. Polanyi, and D. Rogers, J. Chem. Phys. **112**, 11005 (2000).
[20] P. A. Sloan and R. A. Palmer, Nature (London) **434**, 367 (2005).
[21] D. E. Brown, D. J. Moffatt, and R. A. Wolkow, Science **279**, 542 (1998).
[22] S. N. Patitsas, G. P. Lopinski, O. Hul'ko, D. J. Moffatt, and R. A. Wolkow, Surf. Sci. Lett. **457**, 425 (2000).
[23] S. Alavi, R. Rouseau, S. N. Patitsas, G. P. Lopinski, R. A. Wolkow, and T. Siedeman, Phys. Rev. Lett. **85**, 5372 (2000).
[24] B. C. Stipe, M. A. Rezai, and W. Ho, Phys. Rev. Lett. **79**, 4397 (1997).
[25] K. Takayanagi, Y. Tanishiro, M. Takahashi, and S. Takahashi, J. Vac. Sci. Technol. A **3**, 1502 (1985).
[26] R. M. Tromp, R. J. Hamers, and J. E. Demuth, Phys. Rev. B **34**, 1388 (1986).
[27] K. D. Brommer, M. Needels, B. E. Larson, and J. D. Joannopoulos, Phys. Rev. Lett. **68**, 1355 (1992).
[28] K. D. Brommer, B. E. Larson, M. Needels, and J. D. Joannopoulos, Jpn. J. Appl. Phys., Part 1 **32**, 1360 (1993).
[29] K. D. Brommer, M. Galvan, A. D. Pino, Jr., and J. D. Joannopoulos, Surf. Sci. **314**, 57 (1994).
[30] H. Kim, K. Cho, I. Park, J. D. Joannopoulos, and E. Kaxiras, Phys. Rev. B **52**, 17231 (1995).
[31] W. Kern and D. A. Puotinen, RCA Rev. **31**, 187 (1970).
[32] S. A. Horn and S. N. Patitsas, Surf. Sci. **602**, 630 (2008).
[33] J. Tersoff and D. R. Hamann, Phys. Rev. B **31**, 805 (1985).
[34] J. Bardeen, Phys. Rev. Lett. **6**, 57 (1961).
[35] A. Selloni, P. Carnevali, E. Tosatti, and C. D. Chen, Phys. Rev. B **31**, 2602 (1985).
[36] W. Liu, M.S. thesis, University of Lethbridge, 2006.
[37] A constant prefactor on the order of unity has been omitted. See Refs. 33 and 36 for details.
[38] D. A. Papaconstantopoulos, *Handbook of the Band Structure of Elemental Solids* (Springer, New York, 1986).
[39] J. A. Stroscio, R. M. Feenstra, D. M. Newns, and A. P. Fein, J. Vac. Sci. Technol. A **6**, 499 (1988).
[40] J. H. Wilson, D. A. McInnes, J. Knall, A. P. Sutton, and J. B. Pethica, Ultramicroscopy **42**, 801 (1992).
[41] C. E. Housecroft and A. G. Sharpe, *Inorganic Chemistry* (Prentice-Hall, Toronto, 2001), p. 19.
[42] J. M. Pitarke, F. Flores, and P. M. Echenique, Surf. Sci. **234**, 1 (1990).
[43] N. D. Lang, Phys. Rev. B **37**, 10395 (1988).
[44] G. Arfken, *Mathematical Methods for Physicists* (Academic, Toronto, 1985), p. 549.

[45]R. J. Hamers, R. M. Tromp, and J. E. Demuth, Phys. Rev. Lett. **56**, 1972 (1986).
[46]R. Wolkow and Ph. Avouris, Phys. Rev. Lett. **60**, 1049 (1988).
[47]J. J. Boland, Surf. Sci. **244**, 1 (1991).
[48]Th. Fauster and F. J. Himpsel, J. Vac. Sci. Technol. A **1**, 1111 (1983).
[49]F. J. Himpsel and Th. Fauster, J. Vac. Sci. Technol. A **2**, 815 (1984).
[50]R. S. Becker, J. A. Golovchenko, D. R. Hamann, and B. S. Swartzentruber, Phys. Rev. Lett. **55**, 2032 (1985).
[51]P. H. Citrin, J. E. Rowe, and P. Eisenberger, Phys. Rev. B **28**, 2299 (1983).
[52]V. F. Weisskopf and E. Wigner, Z. Phys. **63**, 54 (1930).
[53]W. Voigt, Berl Munch Tierarztl Wochenschr **42**, 603 (1912).
[54]A. B. McLean, C. E. J. Mitchell, and D. M. Swanston, J. Electron Spectrosc. Relat. Phenom. **69**, 125 (1994).